Volume 14
Number 1
January 2021
Pages 1–528

Energy & Environmental Science

rsc.li/ees

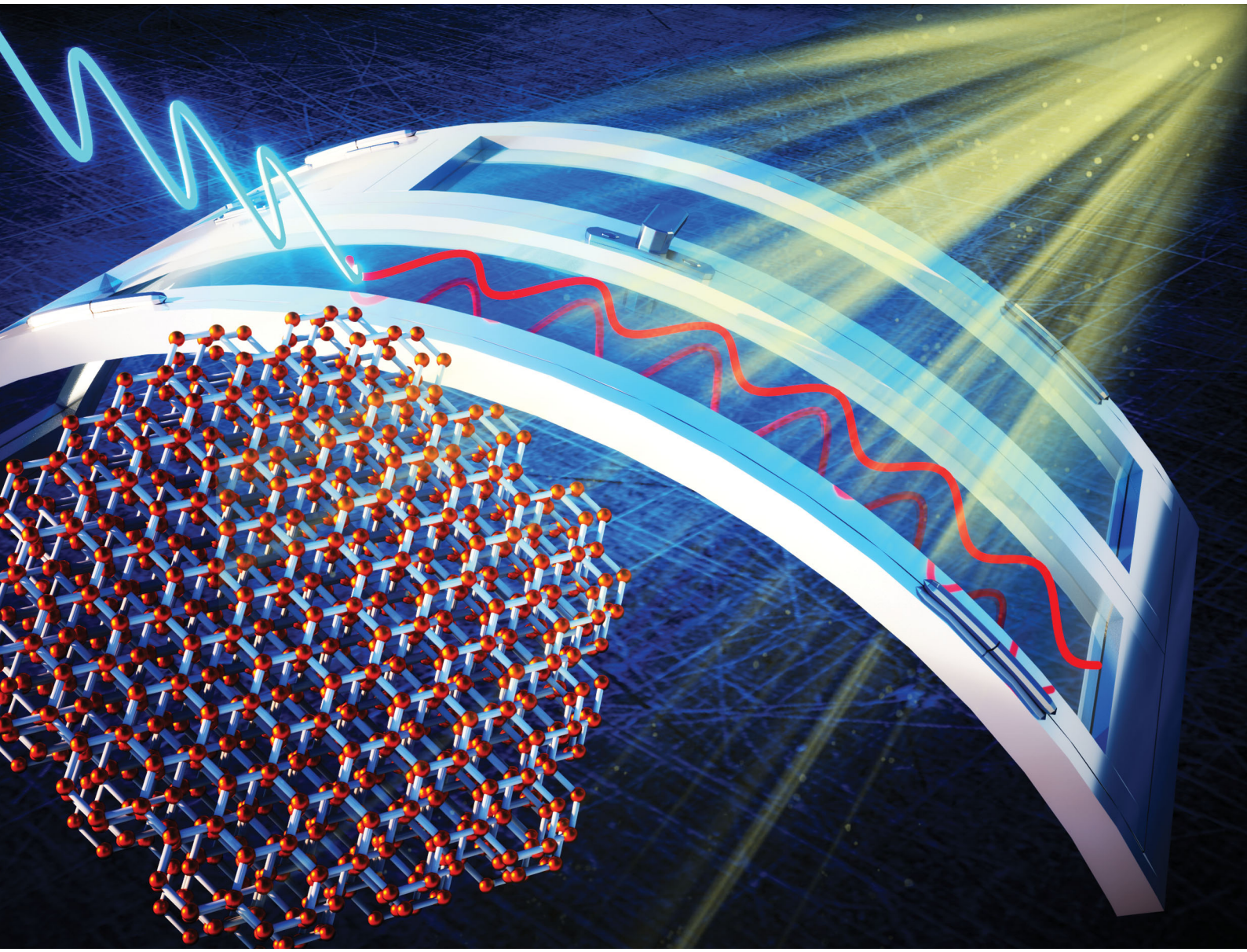

ISSN 1754-5706

ROYAL SOCIETY OF CHEMISTRY

PAPER

Haiguang Zhao, Alberto Vomiero, Xiao Gong *et al.*
Gram-scale synthesis of carbon quantum dots with a large Stokes shift for the fabrication of eco-friendly and high-efficiency luminescent solar concentrators

Energy & Environmental Science

ROYAL SOCIETY OF CHEMISTRY

PAPER

View Article Online
View Journal | View Issue

Cite this: *Energy Environ. Sci.*, 2021, **14**, 396

Gram-scale synthesis of carbon quantum dots with a large Stokes shift for the fabrication of eco-friendly and high-efficiency luminescent solar concentrators†

Haiguang Zhao, *[ab] Guiju Liu,[b] Shujie You,[c] Franco V. A. Camargo, [d] Margherita Zavelani-Rossi, [d] Xiaohan Wang,[ae] Changchun Sun,[ae] Bing Liu,[a] Yuanming Zhang,[a] Guangting Han,[a] Alberto Vomiero *[cf] and Xiao Gong *[g]

Luminescent solar concentrators (LSCs) are large-area sunlight collectors coupled to small area solar cells, for efficient solar-to-electricity conversion. The three key points for the successful market penetration of LSCs are: (i) removal of light losses due to reabsorption during light collection; (ii) high light-to-electrical power conversion efficiency of the final device; (iii) long-term stability of the LSC structure related to the stability of both the matrix and the luminophores. Among various types of fluorophores, carbon quantum dots (C-dots) offer a wide absorption spectrum, high quantum yield, non-toxicity, environmental friendliness, low-cost, and eco-friendly synthetic methods. However, they are characterized by a relatively small Stokes shift, compared to inorganic quantum dots, which limits the highest external optical efficiency that can be obtained for a large-area single-layer LSC (>100 cm^2) based on C-dots below 2%. Herein, we report highly efficient large-area LSCs (100–225 cm^2) based on colloidal C-dots synthesized *via* a space-confined vacuum-heating approach. This one batch reaction could produce Gram-scale C-dots with a high quantum yield (QY) (~65%) using eco-friendly citric acid and urea as precursors. Thanks to their very narrow size distribution, the C-dots produced *via* the space-confined vacuum-heating approach had a large Stokes shift of 0.53 eV, 50% larger than C-dots synthesized *via* a standard solvothermal reaction using the same precursors with a similar absorption range. The large-area LSC (15 × 15 × 0.5 cm^3) prepared by using polyvinyl pyrrolidone (PVP) polymer as a matrix exhibited an external optical efficiency of 2.2% (under natural sun irradiation, 60 mW cm^{-2}, uncharacterized spectrum). After coupling to silicon solar cells, the LSC exhibited a power conversion efficiency (PCE) of 1.13% under natural sunlight illumination (20 mW cm^{-2}, uncharacterized spectrum). These unprecedented results were obtained by completely suppressing the reabsorption losses during light collection, as proved by optical spectroscopy. These findings demonstrate the possibility of obtaining eco-friendly, high-efficiency, large-area LSCs through scalable production techniques, paving the way to the lab-to-fab transition of this kind of devices.

Received 14th July 2020,
Accepted 4th September 2020

DOI: 10.1039/d0ee02235g

rsc.li/ees

[a] *State Key Laboratory of Bio-Fibers and Eco-Textiles, Qingdao University, No. 308 Ningxia Road, Qingdao 266071, P. R. China. E-mail: hgzhao@qdu.edu.cn*
[b] *College of Physics, University Industry Joint Center for Ocean Observation and Broadband Communication, Qingdao University, No. 308 Ningxia Road, Qingdao 266071, P. R. China*
[c] *Division of Materials Science, Department of Engineering Sciences and Mathematics, Luleå University of Technology, 971 87 Luleå, Sweden*
[d] *Dipartimento di Fisica & Dipartimento di Energia, Politecnico di Milano, via G. Ponzio 34/3 and IFN-CNR, piazza L. da Vinci 32, 20133 Milano, Italy*
[e] *College of Textiles & Clothing, Qingdao University, No. 308 Ningxia Road, Qingdao 266071, P. R. China*
[f] *Department of Molecular Science and Nano Systems, Ca' Foscari University of Venice Via Torino 155, 30172 Venezia Mestre, Italy. E-mail: alberto.vomiero@ltu.se*
[g] *State Key Laboratory of Silicate Materials for Architectures, Wuhan University of Technology, 122 Luoshi Road, Wuhan 430070, Hubei, P. R. China. E-mail: xgong@whut.edu.cn*

† Electronic supplementary information (ESI) available. See DOI: 10.1039/d0ee02235g

Broader context

Luminescent solar concentrators (LSCs) are "colored windows" able to generate electric power through light absorption. LSCs represent an elegant solution for semi-transparent or colored facades for so-called building-integrated photovoltaics. Among various types of fluorophores, carbon quantum dots (C-dots) offer a wide absorption spectrum, high quantum yield, environmental friendliness, low-cost, and eco-friendly synthetic methods. The main challenges in developing large-area LSCs based on C-dots come from the low external optical efficiency. In this work, we demonstrate highly efficient large-area LSCs (100–225 cm^2) based on C-dots. The space-confined vacuum-heating approach could produce Gram-scale C-dots with a large Stokes shift of 0.53 eV, and a high quantum yield of ~65%. The LSC (15 × 15 × 0.5 cm^3) exhibited an external optical efficiency of 2.2% (under natural sun irradiation, 60 mW cm^{-2}). After coupling to silicon solar cells, the LSC exhibited a power conversion efficiency of 1.13% under natural sunlight illumination (20 mW cm^{-2}). Compared to inorganic quantum dots and dyes/polymers, the large-scale reaction, low-cost, and the excellent optical properties of the C-dots represent a major advance toward the production of low-cost, high-efficiency, large-area, and scalable LSCs, giving a practical demonstration how the understanding of the optoelectronic features regulating light absorption, emission, and transfer can result in the improved functionality of such devices.

Solar technologies have attracted much attention owing to their sustainable use of sunlight for the production of renewable and clean energy. Solar electricity, solar thermal energy, and solar fuels can contribute to addressing the current energy crisis and climate change issues due to the use of fossil energy.[1–6] Obtaining a high solar-to-electrical power conversion efficiency (PCE) at low cost through solar cells is still a major challenge. Luminescent solar concentrators (LSCs) are large-area sunlight collectors for solar-to-electricity conversion.[4,7,8] An LSC consists of an optical waveguide with embedded fluorophores. Upon illumination, the fluorophores absorb and re-emit light through fluorescence or phosphorescence. Because of the total internal reflection, the emission is guided to edges of the LSC, where a photovoltaic (PV) cell is coupled. The PV cell converts the concentrated emission into electricity. LSC technology can largely decrease the use of expensive PV materials due to the smaller edges of the LSCs compared to its large surface, whereby the PCE of the LSC–PV is over 6%.[4,7,9] In addition, LSCs could be widely used for building integrated PV devices as the typical LSC can be lightweight and semitransparent, with tunable color.[4,7–21] The first proposed LSC dates back more than 40 years ago,[22] but it has not yet reached sufficient maturity to enter the market. The main bottleneck for the mature development of the technology is the strong reabsorption energy loss due to the limited Stokes shift of the fluorophores, because of the overlap between the absorption and emission spectra, which hampers the possibility to obtain a high external optical efficiency. The external optical efficiency is defined as the power of the photons emitted from the LSC edges over the total power of the photons impinging on the LSC through the top surface.[4,7,9] The key to obtaining a high efficiency LSC is to synthesize highly efficient fluorophores, with a broad absorption spectrum, high quantum yield (QY), large Stokes shift, and good stability. It is also very important to balance the efficiency losses in the wavelength shift and PV conversion with the efficiency losses due to the re-scattering of light out of the collector.[23] Ideal fluorophores should have a "uniform absorption cross-section for photons above a threshold energy and constant emissive power in a narrow band from the band-edge energy to the emission peak energy."[23] LSCs experienced very recently a renaissance, thanks to the development of new and highly efficient fluorophores[7] able to guarantee suitable optical properties.

Besides the widely used dyes and polymers, various types of nanocrystals [*e.g.*, inorganic quantum dots (QDs), perovskite nanocrystals, upconversion nanoparticles] have been used as emitters for LSCs.[9,13,15,24–35] Among these, colloidal QDs have attracted a lot of attention due to their size tunable absorption/emission spectra, high absorption coefficient, high QY, size/shape/composition tunable Stokes shift, and good photostability.[7,33,35–38] However, the most efficient QDs used for LSCs either contain toxic Pb or Cd elements [*e.g.*, PbS/CdS, CdSe/CdS, $CsPb(Br_xI_{1-x})_3$, Mn^{2+}-doped $Cd_xZn_{1-x}S$/ZnS] or non-earth-abundant and expensive elements, such as InP/ZnO, CuInS, or CuInS/ZnS.[9,13,15,24–35] Recently earth-abundant Si QDs or carbon QDs (also named as C-dots) have attracted much attention due to their size-tunable absorption, high QY, low-cost, and eco-friendly metal-free composition.[14,26,39–46] Si QDs have an indirect band-gap, which leads to a low absorption coefficient.[44] Thus, they cannot absorb sunlight efficiently. Differently from Si QDs, C-dots have an absorption coefficient comparable to inorganic QDs and have been used as emitters for LSCs.[38–43,47] For example, Talite *et al.* fabricated single-layer small-sized LSCs based on *in situ* cross-linked C-dots with an external optical efficiency of ~12% (LSC dimensions: 3 × 3 cm^2).[42] Due to the large overlap between the absorption and emission of the C-dots, there is strong reabsorption energy loss in large-scale LSCs. Thus, the current reported efficiency in large-area LSCs based on C-dots is still low.[38–42] For example, Zhou *et al.* reported that laminated LSCs based on C-dots exhibited an external optical efficiency of 1.1% (LSC dimensions: 10 × 10 cm^2), which was significantly lower than that of inorganic QDs-based LSCs (2–3% with LSC dimensions: 10 × 10 cm^2).[9,32,34,40] Meanwhile, most of the C-dots were synthesized *via* a solvothermal reaction using nonaqueous solvents, such as dimethylformamide (DMF).[38,41,48] The ideal scenario would be to produce a large quantity of C-dots with z narrow size distribution using eco-friendly precursors and solvents. Very recently, Zhou *et al.* reported the use of a space-confined vacuum-heating approach to produce C-dots in z limited amount and in a rather long process, with a relatively high QY and very narrow size distribution.[49] To the best of our knowledge, there is until now no report on large-area LSCs using narrow-sized C-dots.

In this work, we report highly efficient large-scale LSCs using colloidal C-dots. Based on a space-confined vacuum-heating approach[49] we developed a fabrication procedure that allowed producing Gram-scale C-dots with a high QY (~65%) and large Stokes shift (0.53 eV) using eco-friendly citric acid/urea as precursors and water as the only solvent. The LSC was prepared

by drop-casting a C-dots/polyvinyl pyrrolidone (PVP) polymer solution on glass. The large-area LSC ($15 \times 15 \times 0.5$ cm^3) based on C-dots exhibited an external optical efficiency of 2.2% (under natural sunlight irradiation, 60 mW cm^{-2}), and a PCE of 1.1% under natural sunlight illumination (20 mW cm^{-2}) after coupling to silicon solar cells.

Results and discussion

Synthesis and structure of the C-dots

The C-dots were prepared based on the space-confined vacuum-heating approach using citric acid/urea as precursors and water as the solvent (see the Experimental section)[49] with a key final optimization. For comparison, we also synthesized C-dots through a solvothermal reaction using the same precursors and DMF as the solvent.[41] Briefly, for the Gram-scale synthesis, 1.5 g citric acid, 3 g urea, and 1 g $CaCl_2$ were mixed together and dissolved in 5 mL water. Subsequently, the clear solution was heated to 120 °C under vacuum for 30 min to form a foam structure by pumping away the water. The foam, which forms only in presence of $CaCl_2$, was gradually heated to 250 °C and maintained at this temperature for 1 h. At ~180 °C, the dehydration reaction occurred and C-dots with a light green color were gradually formed through carbonization with further increasing the temperature to 250 °C. The mixture of citric acid, urea, and $CaCl_2$ formed an inflated foam under vacuum heating. The C-dots were formed through dehydration and carbonization processes, which took place in the thin foam walls.[49] Benefiting from the confined space of the foam, the as-synthesized C-dots had a very narrow size distribution (Fig. 1a and b), leading to a uniform energy band gap. By optimizing the ratio between the precursors (citric acid and urea) and the concentration of the precursors (differently from ref. 49), we could obtain over 1 g of purified C-dots for one batch reaction, which presents a good opportunity to produce large-quantity low-cost C-dots for large-scale LSC fabrication. We also mixed the precursors and $CaCl_2$ in water in an identical ratio and dried the mixture at 80 °C for 12 h, to benchmark the space-confined vacuum-heating approach with a standard solvothermal one.[49] The dried foam was then heated to 250 °C. Very-light-green-colored C-dots were obtained, indicating that the vacuum plays a significant role in forming a very uniform foam.

TEM analysis showed that the as-synthesized C-dots fabricated *via* the Gram-scale vacuum-heating approach had a spherical shape with a mean size of 3.6 ± 1.4 nm (Fig. 1a and b). The as-prepared C-dots had a narrower size distribution compared to the C-dots synthesized through the solvothermal reaction (3.9 ± 2.0 nm) (Fig. S1, ESI†). The selected area electron diffraction (SAED) pattern (Fig. 1c) indicated that the C-dots had a hexagonal graphene structure. This was further confirmed by the X-ray diffraction (XRD) pattern as shown in Fig. S2 (ESI†). The broad XRD peak also indicated that the C-dots exhibited a highly defective crystalline structure. The structure of the C-dots was further analyzed by high-resolution TEM (HRTEM), as shown in Fig. 1d. The measured *d* spacing of an individual C-dot was around 2.16 Å, corresponding to the (100) plane of the hexagonal graphene structure,[49,50] which was consistent with the SAED and XRD patterns (Fig. 1c and Fig. S2, ESI†). In the ^{1}H magnetic resonance (NMR) spectrum of the C-dots, peaks appearing in the range of 4–6 indicated the presence of C=C (H) in the C-dots (Fig. S3, ESI†). Usually, C-dots synthesized *via* citric acid/urea have very good water-solubility due to their hydrophilic carboxyl and amide group on the surface.[49–51] The

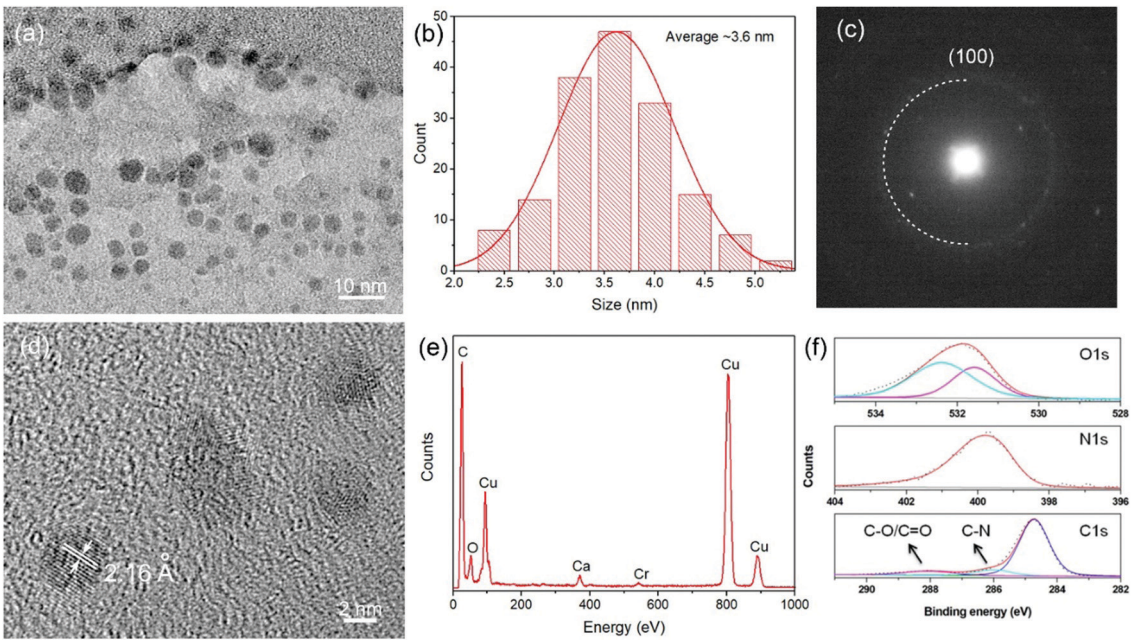

Fig. 1 Typical TEM image (a) and size distribution (b) of the C-dots synthesized *via* the vacuum heating approach. (c) SAED pattern and (d) HRTEM image of the C-dots. (e) EDS of the C-dots. (f) High-resolution XPS spectra of the C-dots.

C═O, C–H, and N–H stretching vibrations observed by FT-IR confirmed the presence of the carboxyl, amide, and hydroxyl groups on the surface of the C-dots (Fig. S4, ESI†).[49–51] The X-ray photoelectron spectroscopy (XPS) results indicated the presence of C, O, N, Cl, and Ca in the C-dots (Fig. S5, ESI†). As shown in Fig. 1f, high-resolution XPS also indicated the formation of C═O, C–OH, and N–H groups in the C-dots, consistent with the FT-IR data.[50] We also found the presence of Ca and Cl in the XPS and energy dispersive X-ray (EDS) spectra (Fig. 1e and f), while no particles were found in the TEM image, indicating that the Ca cations were likely in the form of COOCa.[49]

Optical properties of the C-dots

The C-dots produced by the space-confined vacuum-heating approach dispersed in water (50 mL) had a light-yellow color and exhibited a bright green color under sunlight (Fig. 2d and e). The purified C-dots in methanol had an absorption spectrum covering the 300–500 nm range, which means they can absorb 10% of the total photon energy of the Sun's spectrum (Fig. 2b, top panel). After excitation, the C-dots exhibited a broad photoluminescence (PL) spectrum ranging from 440 to 700 nm with an emission peak located at ~500 nm. Typically, the C-dots synthesized *via* the citric acid/urea *via* solvothermal reaction,[49] with no optimization, had excitation-dependent PL spectra (Fig. S6b, ESI†). Instead, the addition of $CaCl_2$ during the synthesis of the C-dots *via* the vacuum-heating approach resulted in an excitation-independent PL (Fig. 4f), as previously reported in ref. 49, indicating the existence of one type of dominant luminescent center in these C-dots (Fig. 2c). As shown in Fig. S7 (ESI†), with the increase in C-dots concentration from 0.2–1.7 mg mL^{-1}, the integrated PL area almost linearly increased, and then quickly decreased when the concentration was higher than 1.4 mg mL^{-1}. We did not observe any red-shift of the PL peak and broadening of the peak width (Fig. S7b, ESI†). The decrease in the PL intensity at a high C-dot concentration was mainly due to the self-quenching between the neighboring C-dots.[38] These results suggest that we can prepare LSCs with a high C-dots concentration. The as-synthesized C-dots had a QY of (65 ± 3)% in methanol (Fig. S8, ESI†). As a big contrast, the C-dots produced by the solvothermal reaction had a QY of (40 ± 5)%. The much higher QY in the C-dots synthesized *via* the vacuum-heating approach compared to that produced by the solvothermal reaction was due to their lower non-radiative recombination rate, which was further confirmed by the lifetime measurements (Fig. 4h, i and Fig. S6a, ESI†).

The C-dots synthesized *via* the non-vacuum-heating solvothermal approach had a short lifetime of 7.0 ns, which was much shorter than that of 13.1 ns in C-dots produced by the vacuum-heating approach (Table S1, ESI†). The QY can be expressed as:[52]

$$\mathrm{QY} = \frac{k_r}{k_r + k_{nr}} \quad (1)$$

where k_r and k_{nr} are the radiative and the non-radiative decay rates, respectively.

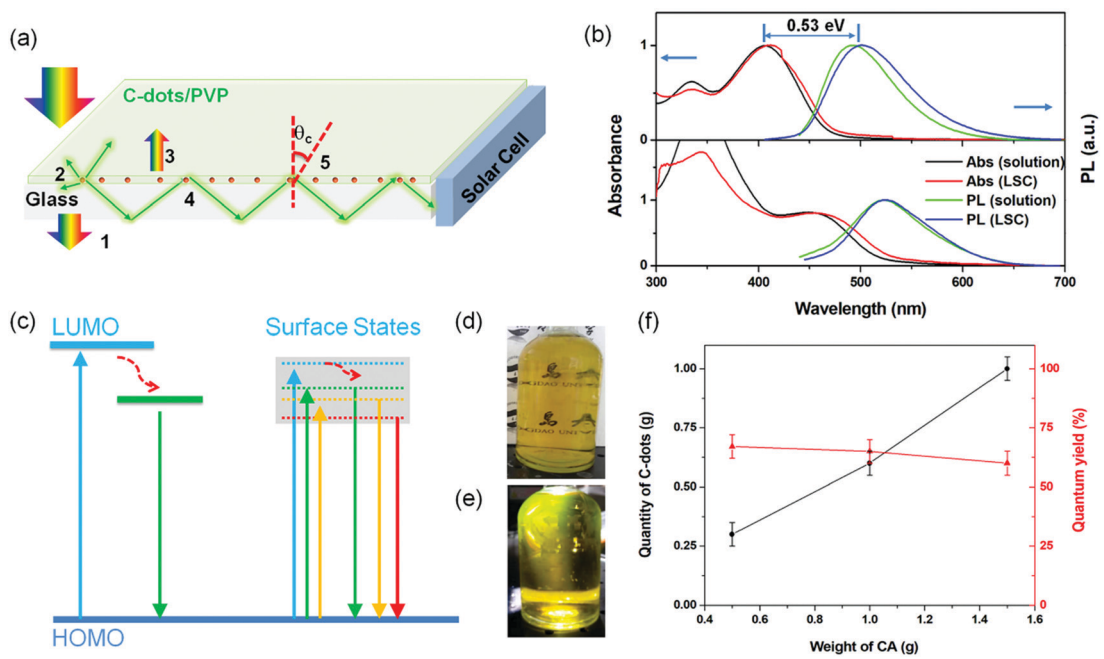

Fig. 2 (a) Schematic representation of a C-dot-based LSC. (b) The absorption and emission spectra of the C-dots produced by the space-confined vacuum heating approach (top panel) and by the standard solvothermal approach (bottom panel), dispersed in methanol or integrated in LSCs. (c) Possible electronic band structure for C-dots produced by space-confined vacuum heating (left) and by the standard solvothermal method (right), which accounts for the large Stokes shift in C-dots produced *via* space-confined vacuum heating. Photography of the C-dots produced by space-confined vacuum heating, dispersed in water (50 mL), under room light (d) or sunlight (e). (f) The obtained QY and quantity of the C-dots produced by the space-confined vacuum heating approach as a function of the citric acid weight.

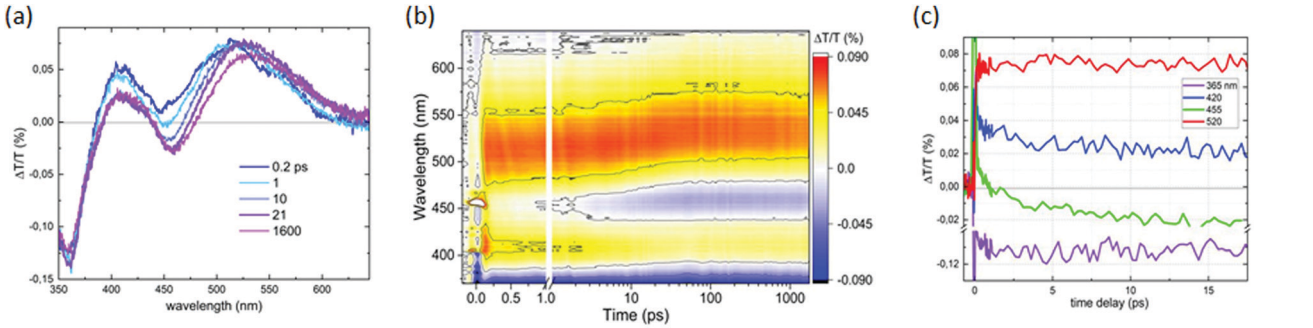

Fig. 3 $\Delta T/T$ spectra of C-dots produced by the space-confined vacuum-heating approach: (a) spectra for selected time delays, (b) map, (c) dynamics for selected wavelengths; pump@400 nm with fluence of 6.5 mJ cm^{-2}, pump and probe polarization are set at magic angle.

The measured lifetime is equal to:

$$\tau = \frac{1}{k_r + k_{nr}} \quad (2)$$

The calculated k_{nr} was 8.6 $\times$ 10^{-8} ns^{-1} in the C-dots synthesized *via* the solvothermal approach, which was three times longer than that in C-dots synthesized *via* the vacuum-heating approach. Both type of C-dots exhibited a similar k_r, indicating a similar surface-energy state dominated radiative recombination mechanism, as widely reported in the literature.[49,53,54] The C-dots synthesized *via* the vacuum-heating approach had a Stokes shift of 0.53 eV, which was larger than that in the C-dots fabricated *via* the solvothermal reaction (0.36 eV) [Fig. 2b (bottom panel)]. We proposed the PL mechanism in both types of C-dots as shown in Fig. 2c. In the C-dots produced by the space-confined vacuum-heating reaction, the recombination of the e–h pairs was through the surface-related energy state with a single type of dominant energy state, different from the band-gap emission, which typically leads to a large Stokes shift.[49,53,54] A similar effect can also explain the large Stokes shift (0.3–0.85 eV) in C-dots reported recently.[54–56] In the C-dots produced *via* the solvothermal reaction, the existence of multiple-recombination centers was due to the not well-passivated surface or the wide size distribution, which often lead to energy transfer,[38,41] explaining also the low QY in the C-dots produced *via* the solvothermal reaction. The optimized space-confined vacuum-heating approach could produce over Gram-scale C-dots in one batch by only increasing the citric acid/urea concentration (Fig. 2f). No significant difference existed in the PL spectra and QYs among the different samples (Fig. 2f and Fig. S9, ESI†).

Optical properties of C-dots

We performed time-resolved transient transmission ($\Delta T/T$) measurements to get insights into the decay channels of the C-dots produced by the space-confined vacuum-heating approach. The excitation pulses were $\sim$100 fs long with a central wavelength at 400 nm, while the probe was a white light continuum spanning from 330 to 660 nm. Fig. 3b shows the $\Delta T/T$ map at low pump fluence (6.5 μJ cm^{-2}), Fig. 3a the corresponding spectra for selected wavelengths, and Fig. 3c the corresponding dynamics for selected probe wavelengths. In the $\Delta T/T$ spectra, two main positive bands appear: the first, centered around 410 nm, which could be assigned to photo-bleaching (PB) of the ground state absorption (see Fig. 2a); the second, peaked at around 520 nm, which was assigned to the stimulated emission (SE) due to its coincidence with the emission spectrum. The negative signal in the short wavelength region came from photoinduced absorption (PIA) to higher excited states. It was interesting to note that at 0.2 ps (dark blue in Fig. 3a), the SE band already shows the spectral features observed in steady state emission. This shows that the Stokes shift in these C-dots took place on a timescale much shorter than 0.2 ps. Throughout our 1.6 ns temporal window, we observed that the SE band did not lose significant intensity, consistent with the high QY and 13 ns lifetime. The only important spectral evolution was observed in the first $\sim$20 ps (see Fig. 3a and c), consisting of a decay of the ground-state PB, the formation of a PIA band around 455 nm and a red-shift of the SE. This is consistent with thermal expansion of the C-dots following the dissipation of the Stokes shift energy.

The expanded lattice showed a red-shifted absorption, explaining the PB recovery at 410 nm and the new PIA band at 455 nm, and this also reduced the gap between the ground and excited states, explaining the SE red-shift. Altogether, the pump–probe showed an ultrafast Stokes shift forming the emissive state in less than 0.2 ps, followed by a single clear radiative decay channel matching the steady state emission. We also noted that the emission did not compete with any PIA, making it very efficient and contributing to the high QY. This behavior is not commonly observed in C-dots.[57,58]

Efficiency of C-dots-based LSCs

LSCs were obtained by mixing the C-dots (synthesized *via* a vacuum heating and solvothermal reaction) with PVP polymer and drop-cast on glass (details in the Experimental section). The typical dimension of the glass for the LSC was 15 $\times$ 15 $\times$ 0.5 cm^3. We targeted the testing of a large-area LSC, because the functional properties in small-area LSCs (typically reported LSC dimensions of 2 $\times$ 2 cm^2 in the literature) are largely overestimated, due to the limited contribution of the reabsorption and scattering losses. In this respect, LSCs represent a special class of devices, where the intrinsic properties of materials have to be tested in a device as close as possible to the real dimensions, otherwise there is a strong risk of significantly overestimating the

optical and power conversion efficiency that can be achieved in the final large-area panels. The average thickness for the polymer/C-dots layer was around 0.5 mm and the mass concentration of C-dots inside the C-dots/PVP film was around 2 wt%, estimated based on the thermal gravity analysis (TGA) (Fig. S10, ESI†).

There was no significant difference in the absorption and emission spectra before and after embedding the C-dots in the polymer film (Fig. 2b). A very slight PL peak position variation of the C-dots in the LSC was detected, most probably due to the change in the refractive index of the matrix (methanol solution *vs.* PVP polymer). The obtained QY of the C-dots in the PVP film was around 67% under 415 nm excitation, consistent with the reported value in the literature.[49] The as-prepared LSC was semitransparent (Fig. 4a–c and Fig. S11, ESI†) under indoor or external natural sunlight (uncharacterized spectra) and simulated sun light (calibrated solar simulator). By irradiating a large-area LSC with a calibrated solar simulator (AM1.5G, 100 mw cm^{-2}), a clear concentrated green light could be seen at the edges of the LSC (Fig. 4b), indicating a great potential for building semi-transparent integrated PVs. This result indicated that there was no QY variation before and after transferring the C-dots from methanol to the PVP polymer matrix, as further confirmed by the transient fluorescence measurement of the PL lifetime. As shown in Fig. 4h and i, the decay time was identical in solution and in the LSC when the samples were excited with a 372 and 445 nm pulsed light-emitting device (LED).

A comparison of the QYs in the solution and solid samples was performed according to the consolidated methodology

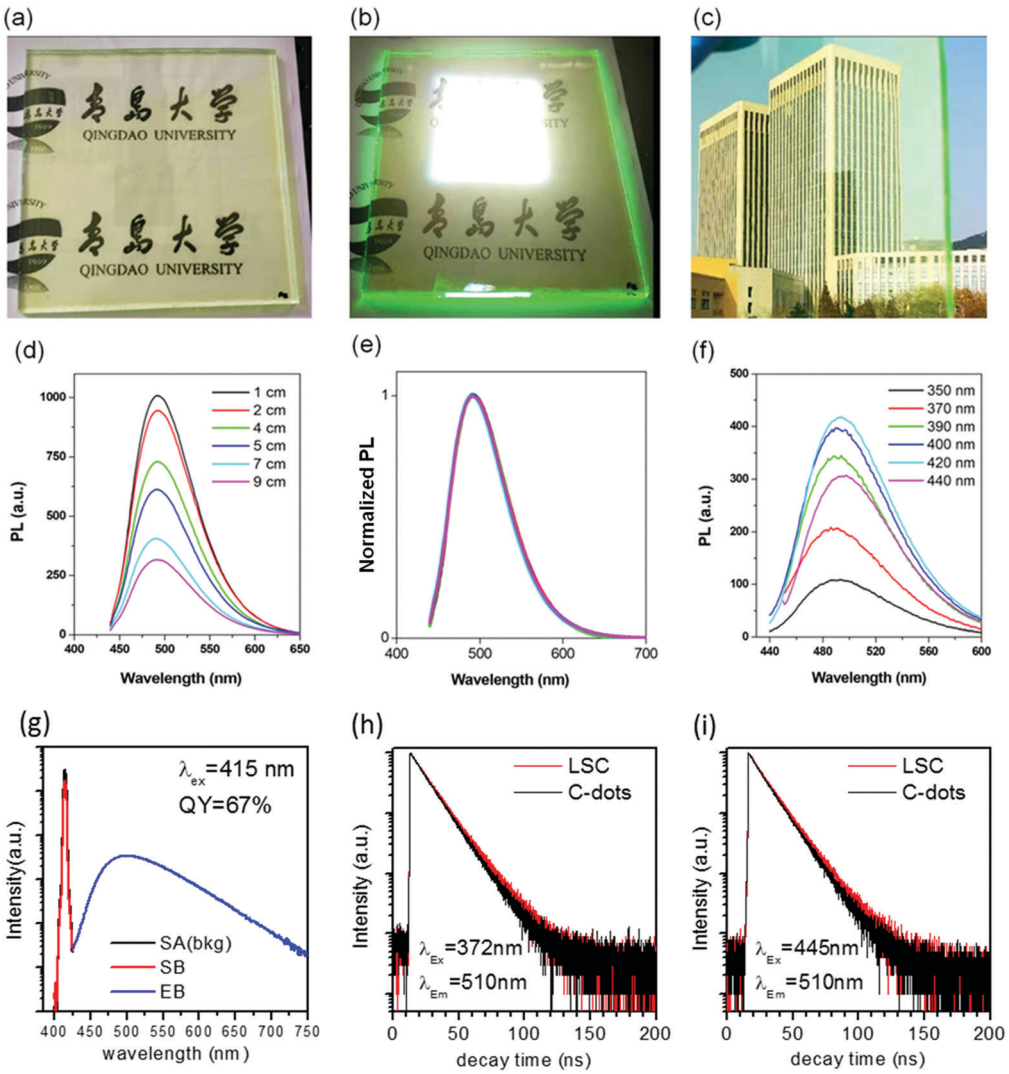

Fig. 4 Photographs of the LSC under indoor (uncalibrated spectrum) (a), simulated sunlight (calibrated solar simulator, AM1.5G, 100 mW cm^{-2}) (b), and natural sunlight (uncalibrated spectrum) illumination (c). PL spectra (d) and normalized PL spectra (e) measured at different optical paths (*L*, distance between the beam spot and the edge of the LSC in the detector direction) for the C-dots-based LSCs. The excitation wavelength was 380 nm. (f) The PL spectra of the C-dots under different excitation wavelengths. The concentration of the C-dots was 2% in the PVP film. The dimensions of the LSC was $15 \times 15 \times 0.5$ cm^3. (g) The scattering and PL emission of LSC (prepared by drop casting) recorded with an integrating sphere. The QY was calculated using the following equation: QY = EB/(SA − SB); SA and SB are the excitation scattering from the integrating sphere and the LSC, respectively; EB is the emission from the LSC. (h and i): The emission decay from C-dots and the LSC excited with a pulsed LED at 372 nm (h) and 445 nm (i).

proposed by Klimov *et al.* (eqn (1) and (2)).[13] As the C-dots had a similar QY and lifetime in solution and in the polymer matrix (LSC), there was almost no variation in k_r and k_{nr}. This result confirmed that the preparation process did not lead to the formation of a significant density of surface-defects/traps, which can highly affect the non-radiative decay rate, k_{nr}, indicating the good stability of the C-dots.

Following the method reported in the literature,[40] we set up the distance-dependent PL measurement as shown in Fig. S12 (ESI†). For the LSC (dimensions of 15 × 15 × 0.5 cm^3, with an optimized C-dots concentration in the polymer film of 2 wt%), the PL intensity of the C-dots decreased with the increase in the distance between the beam spot and edge of the LSC (Fig. 4d). We did not observe any red-shift of the PL spectra (Fig. 4e). Usually, the distance-dependent red-shift of the PL peak position or narrowing of the PL peak width is due to the reabsorption coming from the overlap between the absorption and emission spectra of the C-dots.[40] This phenomenon has been widely reported and used to evaluate the reabsorption energy loss in LSCs.[38,40] In our system, the absence of a PL shift in the LSC with even a high C-dots concentration (2 wt%) was unequivocally attributed to the very large Stokes shift (~0.53 eV) of the C-dots. The working principle and energy loss in an LSC based on C-dots are shown in Fig. 2a. The numbers indicate the major processes in an LSC: (1) transmitted light; (2) partial light loss due to the non-unity of QY; (3) reflected light from the top surface; (4) light re-absorbed and re-emitted by the QDs, with partial losses due to the non-unity of the fluorescence QY (originating re-absorption losses); (5) the critical angle, below which the emitted light will escape from the LSC. The theoretical optical efficiency of an LSC is defined as the number of photons emitted from the LSC edge over the total number of photons impinging on the LSC through the top surface. It can be calculated as:[8]

$$\eta_{opt} = (1 - R)P_{TIR}\cdot\eta_{abs}\cdot\eta_{QY}\cdot\eta_{Stokes}\cdot\eta_{host}\cdot\eta_{self}$$

where R is the reflection of solar light from the waveguide surface, P_{TIR} is the total internal reflection efficiency, η_{abs} is the fraction of solar light that is absorbed by the luminophore, η_{QY} is the QY of luminophore, η_{Stokes} is the energy lost due to heat generation during the absorption and emission event, η_{host} is the transport efficiency of the wave-guided photons through the waveguide, η_{TIR} is the reflection efficiency of the waveguide, and η_{self} is related to re-absorption of the emitted photons by another luminophore in the waveguide.

We calculated the external optical efficiency (η_{opt}) of the LSCs based on the reported method (details included in the Experimental section).[8] In the simulation, the QY of the C-dots in LSCs was set to 65%, and the thickness was fixed as 0.5 mm for the C-dots/PVP layer and 5 mm for the glass. As shown in Fig. 5a, η_{opt} of the as-prepared LSCs using C-dots with a concentration of 2 wt% in the PVP film dropped with increasing the length of the LSC. When L was 100 cm, η_{opt} kept 63% of its initial value. We further measured the η_{opt} of the LSC by coupling a power meter at the edge of the LSC. η_{opt} can be calculated as:[8]

$$\eta_{opt} = \frac{P_{out}\cdot A_{edge}}{P_{in}\cdot A_{LSC}} = \frac{P_{out}}{P_{in}\cdot G}$$

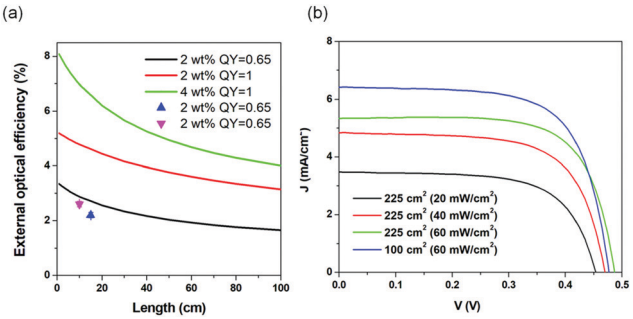

Fig. 5 (a) The calculated external optical efficiency of LSCs based on C-dots with QYs of 65% and 100% with a concentration of 2–4 wt%. The pink and blue triangular markers are the external optical efficiency of the LSCs measured by a power meter for the LSCs with lateral sizes of 100 cm^2 and 225 cm^2, respectively. (b) J–V response of silicon PVs attached on the edge of the LSC under tunable natural sunlight (20–60 mW cm^{-2}).

where P_{out} is the power intensity of the LSC on the edge, P_{in} is the power intensity of the LSC on the surface under direct illumination, A_{edge} is the area of the edges of the LSC, A_{LSC} is the area of the top of the LSC and G was calculated to be 6.8 for the 15 × 15 cm^2, 4.5 for the 10 × 10 cm^2, and 2.5 for the 5 × 5 cm^2 LSC areas.

In the case of large-area LSCs (10 × 10 cm^2 and 15 × 15 cm^2), the power intensity was set at 100 mW cm^{-2} through direct sunlight external illumination, with measuring the light intensity through a calibrated solar cell, but no spectral matching of the light with any standard solar spectrum was guaranteed. In the case of the small-area LSC (5 × 5 cm^2), a calibrated solar simulator was used, where both the light spectrum and intensity were calibrated according to the AM1.5G standard. The measured η_{opt} were 2.7% (G = 4.5) and 2.2% (G = 6.8) for the large-area LSCs, which are consistent with the trend of the calculated optical efficiency of the LSCs with different G or dimensions. We also measured the η_{opt} of the glass/PVP film as a control, which gave a small value of 0.04%, due to the scattering effect of the PVP/glass (Fig. S13, ESI†). The obtained external optical efficiency of the large-area LSC (obtained by applying an uncharacterized spectrum) is the highest ever reported for large-area LSCs (dimensions > 100 cm^2) based on C-dots, thanks to both their high QY and large Stokes shift (Table 1).[38–43]

Theoretically, the optical efficiency can be further improved by enhancing the QY of the C-dots and their absorption, by increasing their concentration in the PVP polymer (Fig. 5a). For example, assuming the C-dots have a QY of 100%, the LSC can exhibit an η_{opt} of 3.19% (L = 100 cm), which is 1.9-time higher than the LSC with the QY of the C-dots of 65%. These results are straightforward evidence that the optical efficiency of LSCs based on C-dots can be largely improved by enhancing the QY of the C-dots. The calculated optical efficiency could reach 4% with an LSC with dimensions of 100 × 100 cm^2 and a QY of 100%, thereby holding great potential for further commercial application.

We measured the PCE of the LSCs by using a calibrated silicon PV cell. The natural sunlight intensity was measured by using a commercial calibrated Zolix QE-B1 solar cell. Under natural sunlight (Qingdao, China), the LSC based on C-dots

Table 1 External optical efficiencies for the LSCs based on different types of fluorophores

LSC	η_{opt} (%)	LSC area (cm^2)	Ref.
C-dots[a]	3.0	25	This work
C-dots[b]	2.7	100	This work
C-dots[b]	2.2	225	This work
NaOH-treated C-dots	1.1	100	41
C-dots[c]	1.6	100	43
N-doped C-dots	3.94	4	59
C-dots[d]	2.3	64	51
C-nanodots	12	9	42
Si QDs	2.85	144	14
CuInS/ZnS QDs	8.1	100	28
CuInS QDs	6.8	900	25
$CuInSe_2$/ZnS	5.1	144	9
Perovskite nanoplatelets	0.87	100	34
CdSe/CdS	1	27.9	28

[a] C-dots were synthesized using a vacuum-heating approach and the external optical efficiency of the LSC was measured under calibrated simulated sunlight (solar simulator AM1.5G, 100 mW cm^{-2}). LSC under internal ambient light (a and b) solar simulator (standard AM1.5G, 100 mW cm^{-2}) and the current density *versus* voltage curve of the LSC are shown in Fig. S14 (ESI). [b] C-dots were synthesized using a vacuum-heating approach and the external optical efficiency of the LSC was measured under natural light (uncharacterized spectrum, 60 mW cm^{-2}, Qingdao, China). [c] C-dots were synthesized using phloroglucinol as a precursor. [d] The LSCs had a tandem structure using three types of C-dots with different absorption wavelengths.

with an active area of 1.6 cm^2 exhibited a typical *J–V* behavior, similar to PVs (Fig. 5b). The LSC with the dimension of 100 cm^2 exhibited a J_{sc} as high as 6.4 mA cm^{-2} (under natural sunlight irradiation in Qingdao, China, 60 mW cm^{-2}), which was 19% higher than the LSC with the dimension of 225 cm^2 under identical measurement conditions. The PCEs of the LSCs were strongly dependent on the natural sunlight intensity. The lower the light intensity, the higher the PCE. This might be due to the decrease in the absorption efficiency of the C-dots at higher light intensity. When the natural sunlight intensity was 20 mW cm^{-2}, the LSC (225 cm^2) exhibited a PCE as high as 1.13%. This indicated that the LSCs based on C-dots are highly suitable to be used in low-light intensity weather (cloudy or morning or late afternoon). Even at a relatively higher natural light intensity (60 mW cm^{-2}, Qingdao, China, winter, noon), the LSCs with dimensions of 100 cm^2 and 225 cm^2 exhibited PCEs of 1.04% and 0.6%, respectively. By big contrast, the LSC fabricated using the solvothermal C-dots exhibited an external optical efficiency of 0.7% because of their strong overlap between the absorption and emission spectra (Table S2, ESI†).

Stability in LSCs

In order to investigate the stability of the C-dots, we measured the PL spectra of the LSCs or C-dots dispersed in solution upon 400 nm illumination (500 mW cm^{-2}) under normal conditions (humidity of 40% at 15 °C). The UV beam spot could cover all of the area in the cuvette (1 × 3 cm^2) and in the LSCs (1 × 1 cm^2). Before the UV-acceleration, the C-dots were dispersed in anhydrous methanol and bubbled with nitrogen for 15 min and the cuvette was sealed. The C-dots concentration in methanol was 1.5 mg mL^{-1} and the mass concentration of C-dots in the PVP film was 2%.

A very slight PL decrease (proportional to the integrated PL area) was recorded for the C-dots dispersed in methanol after 2 h illumination (Fig. 6a and c). By contrast, the C-dots in the LSC exhibited a continuous decrease in the integrated PL area (Fig. 6c), keeping 78% of its initial value. Following the literature,[9] as the absorption of the LSC at (400 ± 5) nm was around 0.5 mW cm^{-2}, we calculated the acceleration factor to be 1000, which translates into 1.4 years of exposure to natural sunlight (average 50 mW cm^{-2} and 8 hour per day). Compared to C-dots dispersed in solution, the solid C-dots have a larger chance to enter into contact with the surrounding environmental conditions.

Under UV-acceleration, the surrounding air or moisture can serve as a quencher, which leads to a decrease in the PL intensity. Usually this quenching will not induce the red-shift of the PL spectra, as we also observed in our experiment (Fig. 6b).[38,41] We also stored the as-prepared LSCs in the dark for 8 months, and found the external optical efficiency of the LSCs fabricated using C-dots synthesized *via* vacuum heating or the solvothermal reaction did not show a significant change, indicating the good stability of the LSCs based on C-dots (Table S2, ESI†). For further improvement of the photostability of the LSC, a laminated structure (where the C-dots/polymer film is placed in between two glass slides) can be used, which can

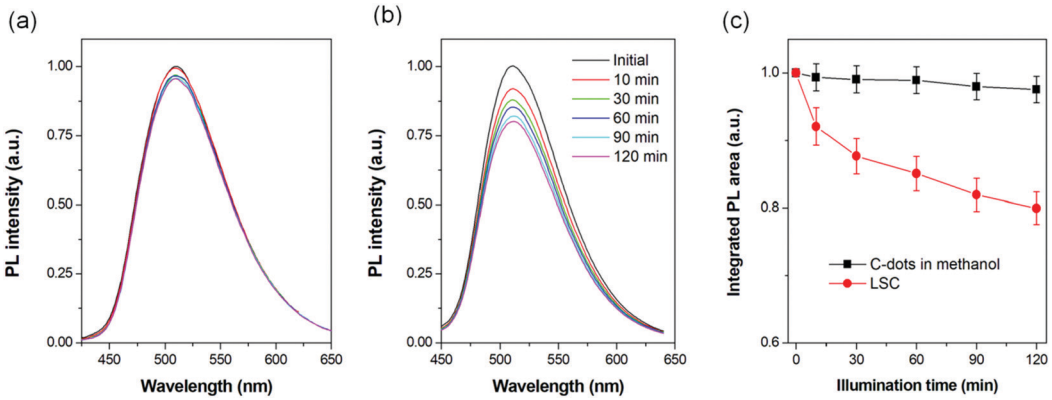

Fig. 6 PL spectra of the C-dots dispersed in methanol (a) and in LSC (b) upon illumination. (c) The integrated PL area of the C-dots upon illumination. The 400-nm illumination had an intensity of 500 mW cm^{-2}.

largely isolate the C-dots from the external environment (air, moisture, or other chemicals).[43]

Conclusions

In summary, we demonstrated a large-area and high-efficiency LSC based on colloidal C-dots with a QY of 65% and a large Stokes shift of 0.53 eV. These peculiar features were derived from the preparation method, which enabled the creation of highly monodispersed and bright dots. The large-area LSC ($15 \times 15 \times 0.5$ cm^3) based on C-dots exhibited a record external optical efficiency of 2.2% for a large-area device (under natural sunlight, uncharacterized spectrum, 60 mW cm^{-2}), and after coupling to silicon solar cells, it exhibited a PCE of 1.13% under natural sunlight illumination (uncharacterized spectrum, 20 mW cm^{-2}). Compared to conventional inorganic QDs and dyes/polymers, the large-scale reaction, low-cost, and the excellent optical properties of the C-dots represent a major advance toward the production of low-cost, high-efficiency, large-area, and scalable LSCs, giving a practical demonstration how the understanding of the optoelectronic features regulating light absorption, emission, and transfer can result in improved functionality of such devices.

These concepts can be generalized also to other structures and devices, where light managing and charge dynamics play a critical role, like, for instance, excitonic solar cells or photoelectrochemical systems for solar fuel production, thus broadening the interest of this study to the general field of optically active nanostructures and composite systems.

Our results highlight an open issue in the LSC community, which is the need to characterize large-area devices through light sources, which are calibrated both in intensity and in spectral matching with the solar spectrum. While natural light calibrated in intensity is becoming familiar to characterize large-area LSCs, a future direction to set a standard in the field would be to find a viable solution to obtain repeatable experiments under standard irradiation conditions, given that large-area solar simulators are far from being available in most research labs worldwide.

Experimental

Synthesis of the colloidal C-dots

The C-dots were prepared *via* a modified space-confined vacuum-heating approach.[49] Typically, 1.5 g citric acid, 3 g urea, and 1 g $CaCl_2$ were mixed together and mixed with 5 mL water. After 10 min sonication, the clear solution was transferred into a 250 mL flask and heated to 120 °C under vacuum for 30 min to pump away the water. At this stage, a foam structure was formed. The foam was gradually heated to 180 °C. After 20 min, the foam was heated to 250 °C and maintained at this temperature for 0.5–1 h. The weight ratio of citric acid/urea was kept at around 2 : 1 with a fixed amount of $CaCl_2$ (1 g). For the reaction with citric acid of 0.5 g and 1 g, the volume of water was kept at 3 mL. The final product was dispersed in ethanol and sonicated for 10 min. Subsequently, the mixture was centrifuged at 8000 g for 10 min. The supernatant was transferred into dialysis bags with a molecular weight of 300 Da for 12 h. Every 2 h, the solution outside of the dialysis bag was replaced with the same volume of water. The C-dots/ethanol solution inside the dialysis bag was collected and dried. The slurry was redispersed in methanol for further characterizations and for use in fabricating LSCs.

Another type of C-dots, for benchmarking purposes, was prepared using a solvothermal method.[41] Typically, citric acid (1 g) and urea (2 g) were dissolved in 10 mL DMF. Subsequently the precursors were transferred into an autoclave and reacted for 6 h at 160 °C. The as-prepared mixture was added dropwise to 50 mL hexane to precipitate the C-dots. The product was then mixed with 20 mL NaOH aqueous solution (50 mg mL^{-1}), stirred for 1 min and centrifuged at 12000 rpm for 30 min.

The precipitates were dispersed in methanol and transferred into dialysis bags with a molecular weight of 3000 Da for 12 h. The solution inside the bag was collected for further characterization and LSC fabrication.

LSC fabrication

A thin film structure was used to fabricate the LSCs.[41] In detail, 10 mL of C-dots methanol solution containing 10–20 mg C-dots, 1 g PVP K30, and 1 g PVP K90 were mixed together. The mixture was sonicated for 10 min in order to obtain a clear solution. The solution was centrifuged at 12 000 rpm for 10 min in order to remove bubbles inside the solution. Then the clear solution was drop-cast on the surface of glasses with different dimensions ($5 \times 5 \times 0.5$ cm^3, $10 \times 10 \times 0.5$ cm^3, $15 \times 15 \times 0.5$ cm^3) and dried at room condition for 1 h until all the solvent was evaporated. The thickness of the C-dots/PVP film was measured to be $\sim$0.5 mm.

Theoretical simulation

The external optical efficiency of the LSCs is expressed as following based on the reported literature:[41]

$$\eta_{\mathrm{opt}} = \eta_{\mathrm{Abs}} \cdot \eta_{\mathrm{internal}} \tag{3}$$

where η_{Abs} is the fraction of absorbed sunlight by the LSC and η_{internal} is the internal quantum efficiency of the LSC.

η_{Abs} can be calculated as:[41]

$$\eta_{\mathrm{Abs}} = \frac{\int_0^{\infty} I_{\mathrm{in}}(\lambda)\left(1 - \mathrm{e}^{-\alpha(\lambda)d}\right)\mathrm{d}\lambda}{\int_0^{\infty} I_{\mathrm{in}}(\lambda)\mathrm{d}\lambda} \tag{4}$$

In which α is the absorption coefficient [calculated as $\alpha = \ln(10)\frac{A}{d}$, where d is the effective length, A is the absorption of the LSC measured by the absorption spectra], and I_{in} is the Sun irradiance. An irradiance corresponding to the AM1.5G standard (100 mW cm^{-2}) was considered, to obtain a fair comparison between the calculations and the experiments carried out by using a calibrated AM1.5G solar simulator as a light source.

A spectrally averaged internal efficiency ($\eta_{internal}$) over the PL emission of the QDs was calculated as:[41]

$$\eta_{internal} = \frac{\int_0^\infty \frac{\eta_{QY} P_{TIR}}{1 + \beta\alpha(\lambda) L_{lsc}(1 - \eta_{QY} P_{TIR})} S_{PL}(\lambda) d\lambda}{\int_0^\infty S_{PL}(\lambda) d\lambda} \quad (5)$$

in which $S_{PL}(\lambda)$ is the PL emission spectrum; β is a numerical value fixed to 1.4, and L_{lsc} is the length of the LSC. Assuming an isotropic emission, P_{TIR} is defined by the escape cone identified by the critical angle θ of the air/glass interface:

$$P_{TIR} = \sqrt{1 - \left(\frac{n_{air}}{n}\right)^2} \quad (6)$$

Characterizations

TEM characterization of the C-dots was carried out using a JEOL 2100F TEM equipped with an EDS spectrometer and SAED. FT-IR (Nicolet 6700), a solution phase NMR (Agilent 600 MHz DD2), and XPS (ESCALAB 250Xi) were used to characterize the surface of the C-dots synthesized *via* a vacuum-heating approach. Typically, the powder C-dots were dispersed in deuterated methanol for 16-scan ^{1}H-NMR measurements. Absorption spectra were acquired with a UV-2600 UV-Vis spectrophotometer (Shimadzu) with a scan speed of 600 nm per minute. PL characterization of the C-dots and the LSCs was performed on an Edinburgh FLS980 instrument. The C-dots were dispersed in methanol with a concentration of 0.05 mg mL^{-1} for the absorption and PL measurements. The QYs of the as-prepared C-dots were measured using Rhodamine 6G as the reference. The time-resolved photoluminescence (TRPL) spectra and QYs of LSCs were recorded with an Edinburgh FLS980 spectrofluorimeter equipped with pulsed LEDs and an integrating sphere. The lifetimes of the C-dots in LSC were obtained with the emission output with the LSC film 45 degrees relative to the detector. The refractive index of glass, PVP/C-dots film was measured using a WAY-2S Albert refractometer (INEA). TGA was carried out in air at 10 °C min^{-1} using a TG209F3 TGA (Netzsch). The pump–probe setup was based on a commercial amplified Ti:Sapphire laser system (Coherent Libra-HE) delivering ~100 fs pulses at 1 kHz repetition rate with a central wavelength of 800 nm. The pump beam at 400 nm was obtained by frequency doubling in a 1 mm-thick β-barium borate crystal and was propagated through a mechanical chopper running at 500 Hz. As a probe pulse, we employed a white light continuum generated in a 3 mm-thick CaF_2 plate. An optical multichannel analyzer then recorded the differential transmission of the probe beam both when the chopper blocked the pump and not. The transient transmission was then computed using $\Delta T/T = (T_{ON} - T_{OFF})/T_{OFF}$ for all the wavelengths of the white light continuum as a function of the pump–probe time delay. The polarization between the pump and probe was set at a magic angle (54.7°) to eliminate the rotational effects. The measurements were performed in a 1 mm pathlength cuvette containing the C-dots dispersed in methanol at ambient temperature.

The external optical efficiency of the large area LSCs was measured under natural light (uncharacterized spectrum, 20–100 mW cm^{-2}, whose intensity was directly measured by using a commercial calibrated Zolix QE-B1 solar cell). The power meter (Newport Model 843-R) was directly coupled on the one edge of the LSC for external optical efficiency measurement. The calibrated PV cell (Zolix QE-B1) was used to measure the PCE of the LSC. The PV cell was coupled directly on one edge of the LSC (active area: 0.55 cm × 2 cm). For the 5 × 5 cm^2 small LSC, the external optical efficiency and the PCE were measured under irradiation from a calibrated solar simulator, NEWPORT, LCS-100 (AM1.5G, 100 mW cm^{-2}). While it was not possible to use a larger area solar simulator as a spectrally and intensity calibrated light source, we report the measurements of both small- and large-area LSC performance. Small-area results are more repeatable, being obtained from a light source calibrated both in intensity and spectral matching with sunlight. However, natural irradiation with an uncalibrated spectrum is becoming more familiar in the LSC community to characterize large-area LSCs.[9] The stability of LSCs or C-dots dispersed in methanol was measured by a PL spectrometer upon illumination (400 nm light emitting device, 500 mW cm^{-2}) in ambient conditions at 20 °C with a humidity of 40%.

Conflicts of interest

There are no conflicts to declare.

Acknowledgements

H. Zhao acknowledges the start funding support from Qingdao University and the funding from the Natural Science Foundation of Shandong Province (ZR2018MB001). S. You and A. Vomiero acknowledge financial support from the Kempe Foundation and the Knut & Alice Wallenberg Foundation.

Notes and references

1 H. Zhao and F. Rosei, *Chem*, 2017, **3**, 229–258.
2 F. Navarro-Pardo, H. Zhao, Z. M. Wang and F. Rosei, *Acc. Chem. Res.*, 2018, **51**, 609–618.
3 H. Zhao, G. Liu, F. Vidal, Y. Wang and A. Vomiero, *Nano Energy*, 2018, **53**, 116–124.
4 Y. Zhou, H. Zhao, D. Ma and F. Rosei, *Chem. Soc. Rev.*, 2018, **47**, 5866–5890.
5 G. Liu, B. Sun, H. Li, Y. Wang and H. Zhao, *J. Mater. Chem. A*, 2019, **7**, 18529–18537.
6 D. Cambie, J. Dobbelaar, P. Riente, J. Vanderspikken, C. Shen, P. H. Seeberger, K. Gilmore, M. G. Debije and T. Noel, *Angew. Chem.*, 2019, **58**, 14374–14378.
7 R. Mazzaro and A. Vomiero, *Adv. Energy Mater.*, 2018, **8**, 1801903.
8 M. G. Debije and P. P. C. Verbunt, *Adv. Energy Mater.*, 2012, **2**, 12–35.
9 K. Wu, H. Li and V. I. Klimov, *Nat. Photonics*, 2018, **12**, 105–110.
10 C. S. Erickson, L. R. Bradshaw, S. McDowall, J. D. Gilbertson, D. R. Gamelin and D. L. Patrick, *ACS Nano*, 2014, **8**, 3461–3467.
11 S.-J. Ha, J.-H. Kang, D. H. Choi, S. K. Nam, E. Reichmanis and J. H. Moon, *ACS Photonics*, 2018, **5**, 3621–3627.

12 F. Meinardi, F. Bruni and S. Brovelli, *Nat. Rev. Mater.*, 2017, **2**, 17085.
13 F. Meinardi, A. Colombo, K. A. Velizhanin, R. Simonutti, M. Lorenzon, L. Beverina, R. Viswanatha, V. I. Klimov and S. Brovelli, *Nat. Photonics*, 2014, **8**, 392–399.
14 F. Meinardi, S. Ehrenberg, L. Dhamo, F. Carulli, M. Mauri, F. Bruni, R. Simonutti, U. Kortshagen and S. Brovelli, *Nat. Photonics*, 2017, **11**, 177–185.
15 S. Sadeghi, H. B. Jalali, R. Melikov, B. G. Kumar, M. M. Aria, C. W. Ow-Yang and S. Nizamoglu, *ACS Appl. Mater. Interfaces*, 2018, **10**, 12975–12982.
16 M. Sharma, K. Gungor, A. Yeltik, M. Olutas, B. Guzelturk, Y. Kelestemur, T. Erdem, S. Delikanli, J. R. McBride and H. V. Demir, *Adv. Mater.*, 2017, **29**, 1700821.
17 L. H. Slooff, E. E. Bende, A. R. Burgers, T. Budel, M. Pravettoni, R. P. Kenny, E. D. Dunlop and A. Buchtemann, *Phys. Status Solidi RRL*, 2008, **2**, 257–259.
18 J. A. H. P. Sol, V. Dehm, R. Hecht, F. Wuerthner, A. P. H. J. Schenning and M. G. Debije, *Angew. Chem.*, 2018, **57**, 1030–1033.
19 J. A. H. P. Sol, G. H. Timmermans, A. J. van Breugel, A. P. H. J. Schenning and M. G. Debije, *Adv. Energy Mater.*, 2018, **8**, 1702922.
20 H.-J. Song, B. G. Jeong, J. Lim, D. C. Lee, W. K. Bae and V. I. Klimov, *Nano Lett.*, 2018, **18**, 395–404.
21 B. R. Sutherland, *Joule*, 2018, **2**, 203–204.
22 J. S. Batchelder, A. H. Zewail and T. Cole, *Appl. Opt.*, 1979, **18**, 3090.
23 H. Hernandez-Noyola, D. H. Potterveld, R. J. Holt and S. B. Darling, *Energy Environ. Sci.*, 2012, **5**, 5798–5802.
24 H. Zhao, D. Benetti, X. Tong, H. Zhang, Y. Zhou, G. Liu, D. Ma, S. Sun, Z. M. Wang, Y. Wang and F. Rosei, *Nano Energy*, 2018, **50**, 756–765.
25 A. Anand, M. L. Zaffalon, G. Gariano, A. Camellini, M. Gandini, R. Brescia, C. Capitani, F. Bruni, V. Pinchetti, M. Zavelani-Rossi, F. Meinardi, S. A. Crooker and S. Brovelli, *Adv. Funct. Mater.*, 2020, **30**, 1906629.
26 X. Gong, W. Ma, Y. Li, L. Zhong, W. Li and X. Zhao, *Org. Electron.*, 2018, **63**, 237–243.
27 G. Liu, R. Mazzaro, Y. Wang, H. Zhao and A. Vomiero, *Nano Energy*, 2019, **60**, 119–126.
28 F. Meinardi, H. McDaniel, F. Carulli, A. Colombo, K. A. Velizhanin, N. S. Makarov, R. Simonutti, V. I. Klimov and S. Brovelli, *Nat. Nanotechnol.*, 2015, **10**, 878–885.
29 M. R. Bergren, N. S. Makarov, K. Ramasamy, A. Jackson, R. Guglielmetti and H. McDaniel, *ACS Energy Lett.*, 2018, **3**, 520–525.
30 B. Zhang, P. Zhao, L. J. Wilson, J. Subbiah, H. Yang, P. Mulvaney, D. J. Jones, K. P. Ghiggino and W. W. H. Wong, *ACS Energy Lett.*, 2019, **4**, 1839–1844.
31 G. Lyu, J. Kendall, E. Preis, S. Baysec, U. Scherf, S. Clement, R. C. Evans and I. Meazzini, *ACS Appl. Polym. Mater.*, 2019, **1**, 3039–3047.
32 H. Zhao, Y. Zhou, D. Benetti, D. Ma and F. Rosei, *Nano Energy*, 2017, **37**, 214–223.
33 G. Liu, H. Zhao, F. Diao, Z. Ling and Y. Wang, *J. Mater. Chem. C*, 2018, **6**, 10059–10066.
34 M. Wei, F. P. G. de Arguer, G. Walters, Z. Yang, L. N. Quan, Y. Kim, R. Sabatini, R. Quintero-Bermudez, L. Gao, J. Z. Fan, F. Fan, A. Gold-Parker, M. F. Toney and E. H. Sargent, *Nat. Energy*, 2019, **4**, 197–205.
35 H. Zhao, R. Sun, Z. Wang, K. Fu, X. Hu and Y. Zhang, *Adv. Funct. Mater.*, 2019, **29**, 1902262.
36 Y. You, X. Tong, W. Wang, J. Sun, P. Yu, H. Ji, X. Niu and Z. M. Wang, *Adv. Sci.*, 2019, **6**, 1801967.
37 Z. Li, X. Zhao, C. Huang and X. Gong, *J. Mater. Chem. C*, 2019, **7**, 12373–12387.
38 H. Zhao, *J. Lumin.*, 2019, **211**, 150–156.
39 W. Ma, W. Li, R. Liu, M. Cao, X. Zhao and X. Gong, *Chem. Commun.*, 2019, **55**, 7486–7489.
40 Z. Wang, X. Zhao, Z. Guo, P. Miao and X. Gong, *Org. Electron.*, 2018, **62**, 284–289.
41 Y. Zhou, D. Benetti, X. Tong, L. Jin, Z. M. Wang, D. Ma, H. Zhao and F. Rosei, *Nano Energy*, 2018, **44**, 378–387.
42 M. J. Talite, H.-Y. Huang, Y.-H. Wu, P. G. Sena, K.-B. Cai, T.-N. Lin, J.-L. Shen, W.-C. Chou and C.-T. Yuan, *ACS Appl. Mater. Interfaces*, 2018, **10**, 34184–34192.
43 H. Zhao, G. Liu and G. Han, *Nanoscale Adv.*, 2019, **1**, 4888–4894.
44 R. Mazzaro, A. Gradone, S. Angelon, G. Morselli, P. G. Cozzi, F. Romano, A. Vomiero and P. Ceroni, *ACS Photonics*, 2019, **6**, 2303–2311.
45 W. Ma, W. Li, M. Cao, R. Liu, X. Zhao and X. Gong, *Org. Electron.*, 2019, **73**, 226–230.
46 E. Bladt, R. J. A. van Dijk-Moes, J. Peters, F. Montanarella, C. D. M. Donega, D. Vanmaekelbergh and S. Bals, *J. Am. Chem. Soc.*, 2016, **138**, 14288–14293.
47 M. J. A. Talite, H.-Y. Huang, K.-B. Cai, K. C. C. Co, P. A. C. Santoso, S. H. Chang, W.-C. Chou and C.-T. Yuan, *J. Phys. Chem. Lett.*, 2020, **11**, 567–573.
48 Z. Wang, F. Yuan, X. Li, Y. Li, H. Zhong, L. Fan and S. Yang, *Adv. Mater.*, 2017, **29**, 1702910.
49 D. Zhou, P. Jing, Y. Wang, Y. Zhai, D. Li, Y. Xiong, A. V. Baranov, S. Qu and A. L. Rogach, *Nanoscale Horiz.*, 2019, **4**, 388–395.
50 K. Hola, M. Sudolska, S. Kalytchuk, D. Nachtigallova, A. L. Rogach, M. Otyepka and R. Zboril, *ACS Nano*, 2017, **11**, 12402–12410.
51 L. Zdražil, K. Hola, M. Petr, O. Zmeškal, S. Kment, A. Rogach and R. Zboril, *Nanoscale*, 2020, **12**, 6664–6672.
52 P. G. Seybold, M. Gouterman and J. Callis, *Photochem. Photobiol.*, 1969, **9**, 229–242.
53 S. Qu, D. Zhou, D. Li, W. Ji, P. Jing, D. Han, L. Liu, H. Zeng and D. Shen, *Adv. Mater.*, 2016, **28**, 3516–3521.
54 Y. Choi, B. Kang, J. Lee, S. Kim, G. T. Kim, H. Kang, B. R. Lee, H. Kim, S. Shim, G. Lee, O. Kwon and B. Kim, *Chem. Mater.*, 2016, **28**, 6840–6847.
55 Y. Zhang, X. Liu, Y. Fan, X. Guo, L. Zhou, Y. Lv and J. Lin, *Nanoscale*, 2016, **8**, 15281–15287.
56 H. Jia, Z. Wang, T. Yuan, F. Yuan, X. Li, Y. Li, Z. Tan, L. Fan and S. Yang, *Adv. Sci.*, 2019, **6**, 1900397.
57 L. Z. Sui and W. W. Jin, *Phys. Chem. Chem. Phys.*, 2016, **18**, 3838–3845.
58 A. Sciortino, A. Cannizzo and F. Messina, *J. Carbon Res. C*, 2018, **4**, 67.
59 Y. Li, P. Miao, W. Zhou, X. Gong and X. Zhao, *J. Mater. Chem. A*, 2017, **5**, 21452–21459.

